Acetazolamide Challenge Changes Outer Retina Bioenergy-Linked and Anatomical OCT Biomarkers Depending on Mouse Strain

Bruce A. Berkowitz,[1] Anuhya Paruchuri,[1] Josh Stanek,[1] Robert H. Podolsky,[2] Karen Lins Childers,[3] and Robin Roberts[1]

[1]Department of Ophthalmology, Visual and Anatomical Sciences, Wayne State University School of Medicine, Detroit, Michigan, United States
[2]Biostatistics and Study Methodology, Children's National Hospital, Silver Spring, Maryland, United States
[3]Beaumont Research Institute, Beaumont Health, Royal Oak, Michigan, United States

PURPOSE. The purpose of this study was to test the hypothesis that optical coherence tomography (OCT) bioenergy-linked and anatomical biomarkers are responsive to an acetazolamide (ACZ) provocation.

METHODS. C57BL/6J mice (B6J, a strain with relatively inefficient mitochondria) and 129S6/ev mice (S6, a strain with relatively efficient mitochondria) were given a single IP injection of ACZ (carbonic anhydrase inhibitor) or vehicle. In each mouse, the Mitochondrial Configuration within Photoreceptors based on the profile shape Aspect Ratio (MCP/AR) index was determined from the hyper-reflective band immediately posterior to the external limiting membrane (ELM). In addition, we tested for ACZ-induced acidification by measuring contraction of the external limiting membrane-retinal pigment epithelium (ELM-RPE) thickness; the hyporeflective band (HB) signal intensity at the photoreceptor tips was also examined. Finally, the nuclear layer thickness was measured.

RESULTS. In response to ACZ, MCP/AR was greater-than-vehicle in B6J mice and lower-than-vehicle in S6 mice. ACZ-treated B6J and S6 mice both showed ELM-RPE contraction compared to vehicle-treated mice, consistent with dehydration in response to subretinal space acidification. The HB intensity at the photoreceptor tips and the outer nuclear layer thickness (B6J and S6), as well as the inner nuclear layer thickness of B6J mice, were all lower than vehicle following ACZ.

CONCLUSIONS. Photoreceptor respiratory efficacy can be evaluated in vivo based on distinct rod mitochondria responses to subretinal space acidification measured with OCT biomarkers and an ACZ challenge, supporting and extending our previous findings measured with light-dark conditions.

Keywords: photoreceptor, optical coherence tomography (OCT), biomarker, mitochondria, energy, acidification

Retinal pH is a major regulator of rod function and visual performance.[1–10] For example, subretinal space hydration – and the distribution of components within the subretinal space (e.g. interphotoreceptor binding protein [IRBP]) is controlled by pH.[6,11,12] Photoreceptors normally produce substantial waste water acidified by CO_2 and lactate under high energy demand conditions, such as maintaining the dark current, and this acidified water is effectively removed by upregulation of pH-sensitive co-transporters on the apical retinal pigment epithelium (RPE).[6,12–14] Low outer retina pH – such as that measured, for example, early in the course of experimental diabetic retinopathy – is also expected to modify mitochondria dynamics to maintain cell functioning and survival based on cell culture studies.[15,16] However, it is unclear if this low pH – mitochondria configuration signaling pathway occurs in photoreceptors in vivo. Addressing this question will help in the development of therapies against prolonged acidification of the retina and its sight-threatening consequences of retinal dysfunction, degeneration, and / or neovascularization.[14,17–20]

We have discovered that the Mitochondria Configuration within Photoreceptors can be measured by the profile shape Aspect Ratio (MCP/AR) of the optical coherence tomography (OCT) hyper-reflective band posterior to external limiting membrane (ELM).[21,22] Confirmatory electron microscopy and oxygen consumption rate measurements support MCP/AR as a noninvasive index of mitochondria activity/distribution in C57BL/6J mice.[21,22] In addition, we and others have shown the ELM – RPE thickness is sensitive to reductions in pH. For example, normal, low pH conditions (e.g. during dark-adaptation) upregulate co-transporters on apical RPE that dehydrate the subretinal space causing ELM-RPE contraction.[6,23,24] Retinal acidification can also be produced by a systemic injection of the carbonic anhydrase

inhibitor acetazolamide (ACZ) and is also associated with a reduced ELM-RPE thickness.[23,25,26] Carbonic anhydrase facilitates the reversable hydration of carbon dioxide to carbonic acid, which then dissociates to bicarbonate and hydrogen ions thus helping to regulate intra- and extracellular pH. ACZ is used to lower intraocular pressure and, in imaging studies, provides a neurovascular reactivity challenge that is useful in clinical neurology and ophthalmology.[27,28] It is unclear how rod MCP/AR changes in response to ACZ-evoked reduction in pH.

In this study, we test the hypothesis that an acute systemic injection of ACZ in mice alters the MCP in vivo. Further, we examine how baseline mitochondria efficacy modifies this response by comparing the OCT biomarker responses to ACZ in C57BL/6J (B6J) and 129S6/ev (S6) mice. B6J mice lack the mitochondria nicotinamide nucleotide transhydrogenase (*Nnt*) gene, a mutation not reported for S6 mice, and thus B6J mice have less efficient mitochondria than S6 mice.[29] Specifically, compared to S6 mice, B6J mice show an 11% lower mitochondria maximum reserve capacity (an index of activity/efficacy of mitochondrial function in the generation of ATP per unit of consumed oxygen),[10,30,31] larger light-dark changes in MCP/AR,[21] greater light-dark ELM-RPE thickness differences,[10,23] larger posterior retina hydration differences,[10] and a higher production of free radicals and greater susceptibility to neurodegeneration from sodium iodate.[32-34]

METHODS

All mice were treated in accordance with the National Institutes of Health Guide for the Care and Use of Laboratory Animals, the Association for Research in Vision and Ophthalmology Statement for the Use of Animals in Ophthalmic and Vision Research, and with specific authorization by the Wayne State University Division of Laboratory Animal Resources Institutional Animal and Care Use Committee (IACUC). For the OCT studies performed at Wayne State University, 2 month old male C57BL/6J mice (B6J; $n = 10$; Jackson Laboratories, Bar Harbor, ME, USA), and male 129S6/ev mice (S6; $n = 10$; Taconic Laboratories, Rensselaer, NY, USA) were housed and maintained in 12-hour/12-hour light-dark cycle laboratory lighting. After scanning, mice were humanely euthanized by an overdose of ketamine/xylazine followed by cervical dislocation, per our Wayne State University Institutional Animal and Care Use Committee–approved protocol. Data in this study were collected from the left eye to minimize potential left-right eye differences between groups and to allow for comparisons with our previous results.

Acetazolamide Dosing

Dark-adapted mice were given intraperitoneal injections of either 250 mg/kg ACZ (pH 9) or phosphate buffered saline (vehicle, equal volume, pH 9) approximately 2 hours before light adaptation. Mice were then examined by OCT either 1 (B6J and S6 mice) or 5 hours (B6J mice only) after light adaptation.

Optical Coherence Tomography

In this study, we used a cross-sectional design in which anesthetized mice—100 mg/kg ketamine (Covetrus, Port-land, ME, USA) and 6 mg/kg xylazine (MWI Animal Health, Boise, ID, USA)—were examined by OCT (Envisu UHR2200; Bioptigen, Durham, NC, USA) in the morning (i.e. before noon). Mice were dark adapted overnight, and the following day, room-light adapted for just 1 hour or 5 hours (B6J only) prior to imaging. To dilate the iris, 1% atropine sulfate was used, and Systane Ultra (Alcon, Geneva, Switzerland) was used to lubricate the eyes.

From the central retina, we collected radial volume scans with following parameters: A-scans/B-scans = 1000 lines; B-scans/volume = 1000 scans; and frames/B-scan = 1 frame. To minimize the effects of noise, and boost the signal, 100 images are registered and averaged before being analyzed. These 100 images were extracted from B-scan numbers 450 to 549 (representing inferior–superior retina) were registered (in-house script for R; R Foundation for Statistical Computing, Vienna, Austria). Briefly, first-pass rigid body registration with RNiftyReg (function in R) was used to rotate the image and interpolate signal at each pixel. Next, non-rotational rigid-body approaches (at the level of a given row or column of pixels) were applied three times. The 100 images were visually compared as a final step before averaging. A representative image of the outer retina and a set of axial reflectance profiles are shown in Figure 1.

Image Analysis

Laminar boundaries for segmentation were estimated with a previously described machine learning model–based computer program.[11] Briefly, the machine learning model was a U-net convolutional neural network trained using the "dice loss" function and the Adam optimizer (learning rate = 0.001), with 665 previously labeled images for training and 166 and 356 images for validation and testing, respectively. To improve the performance of the model, its predictions were postprocessed by applying a shortest-path algorithm. From the model-based estimates, segmentation was then performed with an R script. The intensity values used to generate the EZ reflectivity profile shape are measured from a log-based image with a 16-bit depth (default in the Bioptigen system). Previously, we compared images before and after converting them from log to linear values using a simple, empirically derived equation and noted that EZ reflectivity profile shape differences would be detected with either output; more detailed work in this area is warranted.

Once segmented, inferior and superior retinas (350–624 µm from the optic nerve head on the inferior and superior sides) were each analyzed; starting at 350 µm ensured that our data were analyzed away from the optic nerve head, where the outer retina is relatively uniform in all OCT data. We measured the ELM-RPE thickness from in-house R scripts that objectively extracted layer boundaries obtained after searching the space provided by a machine-learning estimates ("seed boundaries") as above. The ELM and RPE are initially identified by local signal maxima and the R script determine the ELM-RPE thickness by calculating the distance from ELM to the basal side of the RPE at the level of Bruch's membrane.[35-37]

The magnitude of the relative HB signal intensity is calculated, as previously described, by analyzing profile contours spanning the reflectance peak of the RPE and outer segment tips. A straight line is drawn between the RPE and the outer
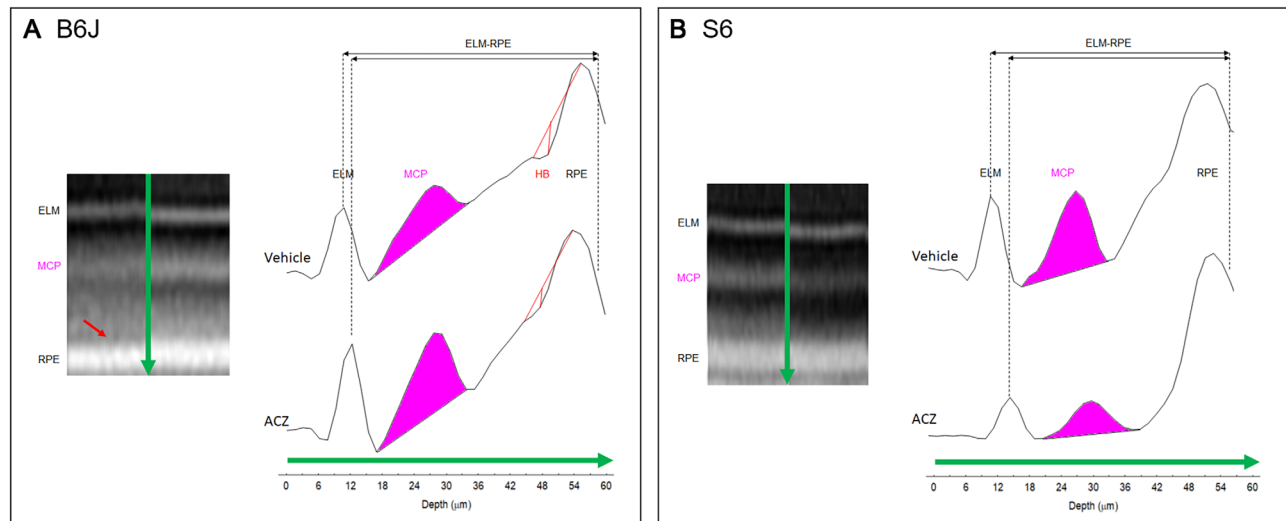
FIGURE 1. Summary of qualitative changes in representative OCT data from vehicle or ACZ-treated 1 hour light-adapted (**A**) B6J and (**B**) S6 mice. Example OCTs of the outer retina are shown on the left side of each panel; within this panel vehicle treated mice on the *left side* of the *green arrow* and ACZ treated mice are on the *right side*. ELM, external limiting membrane; region from which the mitochondrial configuration within photoreceptors (MCP; *pink*) is measured; RPE, retinal pigment epithelium; HB intensity (*red arrow* and *lines*). On the *right side* of each panel, representative reflectivity (or signal intensity) profile, also known as the A-line (*green arrow*) are shown; these A-line profiles are scaled the same; no y-axis is shown because units are arbitrary. No signal intensity normalization was performed. Note HB is not measurable /clearly defined in S6 mice; that is the reflectance dip seen just anteriorly to the RPE band at the photoreceptor tips in (**A**) is not well defined in (**B**).[23]

segment tip portions of the profile (intersecting only one point on each side of the HB) and the largest departure from that line is the magnitude of the relative HB signal intensity; the magnitude of this decrease in reflectivity/intensity is presented herein.[23,38,39]

Our analysis generated the following outputs: (1) a spreadsheet of distances from the optic nerve head and layer thickness, and (2) a spreadsheet containing the HB magnitude. The output image had the basal aspect of the RPE held in a fixed position without stretching the image; this non-stretched image was used to generate the A-line reflectivity profiles shown in Figure 1.

We analyzed MCP/AR using an unbiased approach in which MATLAB code (MathWorks, Natick, MA, USA) determines the baseline for hyper-reflective band immediately posterior to the ELM. The profile shape descriptor for this reflectivity profile was generated using the Fit Ellipse command in ImageJ. In the results window, the value under the column marked "round" is the minor-to-major aspect ratio for the fitted ellipse, termed herein as MCP/AR; this process is described at https://imagej.nih.gov/ij/source/ij/process/EllipseFitter.java and more formally in the literature.[40] It remains to be determined if the ellipse aspect ratio, a commonly used shape descriptor; is an optimal shape description for these types of studies, nonetheless it remains useful.[21,22,41] In addition, our experience to date is that MCP/AR is not a function of ELM-RPE thickness, an impression supported by the data in this report (see below). Any potential bias in MCP/AR due to noise was not considered.

Statistical Analyses

Data are presented as mean and 95% confidence intervals, and we used $P < 0.05$ for all analyses. We used linear mixed models with the Kenward-Roger method for calculating degrees of freedom in SAS version 9.4 (SAS Software,

Cary, NC, USA) to analyze all measurements. We first averaged all values for all variables across depth/distance separately for each side (inferior/superior). We analyzed B6J and S6 mice separately. For B6J mice, we used a linear mixed model that included the fixed effects of treatment (ACZ versus vehicle), time of light adaptation, side, and all interactions, whereas we used only treatment, side, and the treatment by side interaction for S6 mice. All models included a random intercept for subject within group (treatment/time combination for B6J or treatment for S6). Using these initial models, we first evaluated the highest order interactions, removing any interactions that were not significant to arrive at a final model.

RESULTS

OCT Energy Biomarkers

As summarized in Figures 1 and 2, MCP/AR was greater in B6J mice (regardless of duration of light adaptation) but smaller in S6 mice in response to an ACZ provocation. Both strains, however, showed a contracted ELM-RPE after ACZ. In addition, the HB intensity becomes smaller following ACZ in B6J mice; it is hard to discern a similar HB region-of-interest just anteriorly to the RPE band in S6 mice, as noted previously.[23]

OCT Laminar Biomarkers

As summarized in Figure 3, ACZ reduced ONL thickness in B6J and S6 mice after 1 hour of light adaptation. In addition, the inner nuclear layer (INL) + outer plexiform layer (OPL) layer contracted following ACZ in B6J after either 1 or 5 hours of light adaptation but not in S6 mice after 1 hour of light adaptation. Neither strain demonstrated a change in the IPL with ACZ.
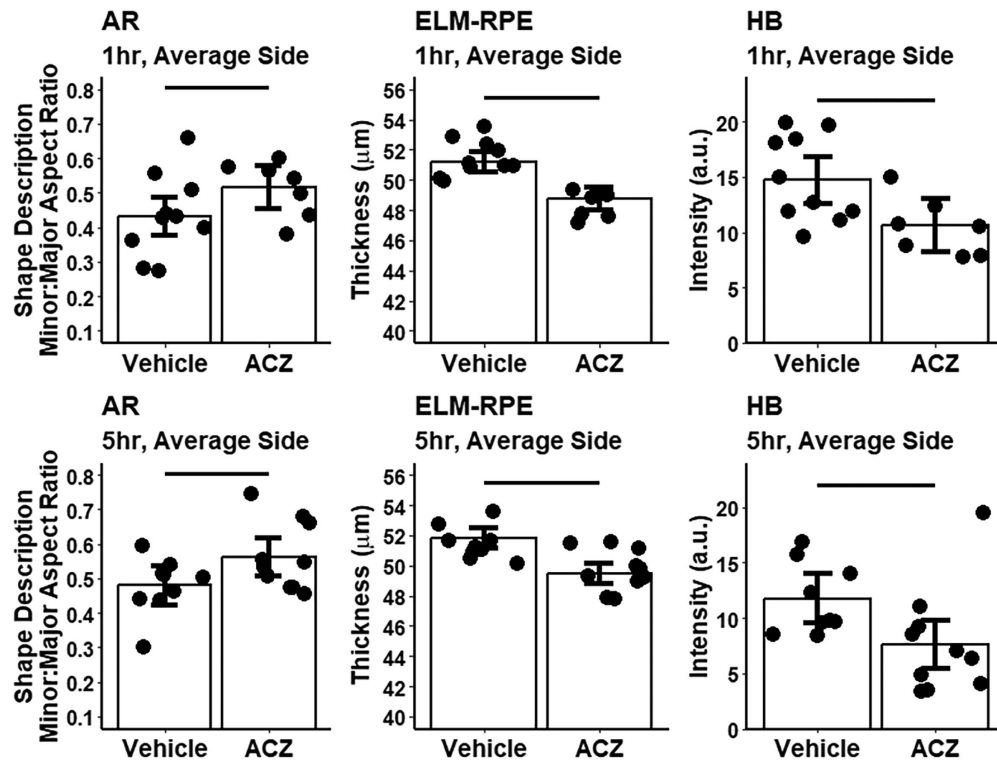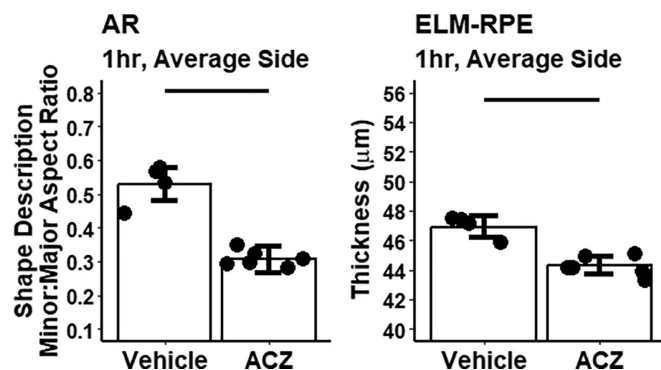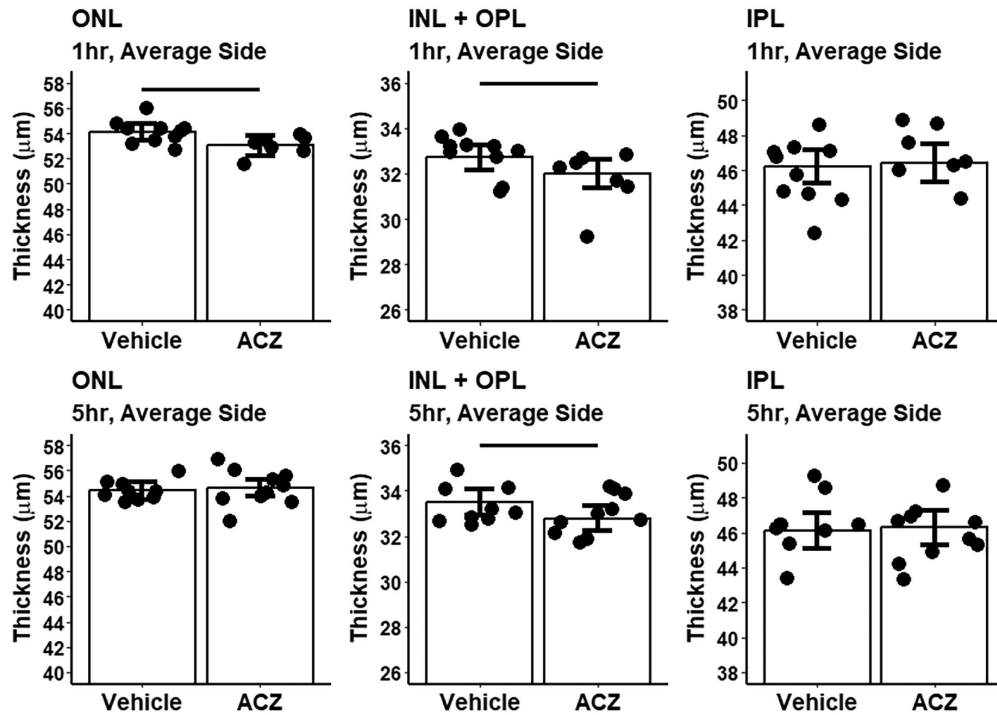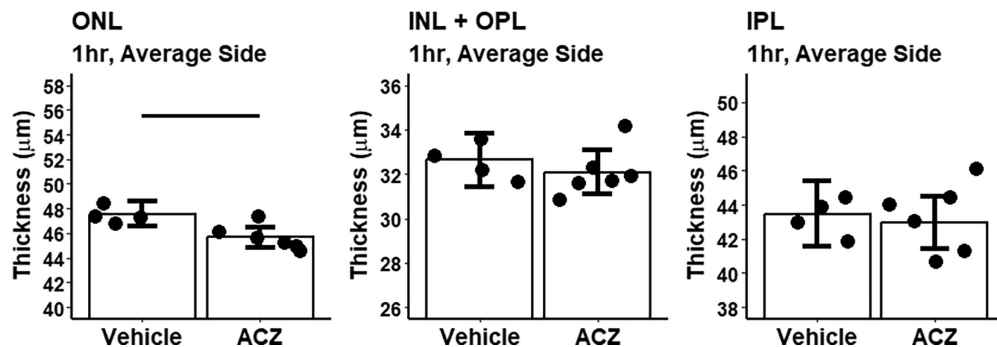
FIGURE 2. Summary of quantitative changes in energy biomarkers from vehicle or ACZ-treated light-adapted (**A**) B6J and (**B**) S6 mice. Same graph conventions as in Figure 1 are used. *Black horizontal line* indicates $P < 0.05$ (two-tailed, linear mixed-model analysis; mean $\pm$ 95% confidence interval [CI]). Individual data points represent the measured value for each mouse. Note HB is not measurable/clearly defined in S6 mice (see Fig. 1).[23] No differences between inferior and superior retina were noted and average side results are shown.

DISCUSSION

In this study, MCP/AR was shown to be sensitive to an ACZ challenge. Further, the two mouse strains examined seem to use distinct approaches to preserve their function and survival during ACZ-induced acidification. B6J mice, a strain with mitochondrial redox abnormalities, increases its energy output – and acidifies the subretinal space – while maintaining the dark current accompanied by a change in mitochondrial distribution that increases MCP/AR. The MCP/AR also increases in B6J mice after the ACZ provocation (see Fig. 1); this was observed after 1 hour or 5 hours of ACZ (thus, we focused on the 1 hour time point for the S6 mice).[21,29] On the other hand, S6 mice, a strain with more efficient

mitochondria than in B6J mice, did not previously show changes in mitochondrial distribution with increases in rod energy output in the dark and its related acidification of the subretinal space. However, S6 mice following ACZ show a lower-than-vehicle MCP/AR, a response not seen in light-dark conditions where MCP/AR remained constant, perhaps as a consequence of the relatively lower pH produced by ACZ than with dark.[21,25,42] The ACZ-evoked decrease in MCP/AR in S6 mice suggests a more elongated distribution of mitochondria within the ellipsoid than in B6J mice.[21] The underlying mechanism is unclear at present but we note that low pH conditions cause mitochondria in neurons to elongate.[15] If this happens in rods of S6 mice, elongation could contribute to an apparent change in mitochondria distribu-

A B6J

B S6

FIGURE 3. Summary of quantitative changes in layer thickness biomarkers from vehicle or ACZ-treated light-adapted (**A**) B6J and (**B**) S6 mice. Same graph conventions as in Figure 1 are used, in addition INL + OPL, the combined thickness of the inner nuclear layer and outer plexiform layer; IPL, inner plexiform layer. *Black horizontal line* indicates $P < 0.05$ (two-tailed, linear mixed-model analysis; mean $\pm$ 95% confidence interval [CI]). Individual data points represent the measured value for each mouse. No differences between inferior and superior retina were noted and average side results are shown.

tion indicated by a lower MCP/AR. More studies are needed to test these notions.

Nonetheless, we note that ACZ-evoked ELM-RPE contraction, the expected consequence of low pH upregulation of apical RPE water removal co-transporters.[5,6,23] Subretinal space contraction by ACZ had been first observed noninvasively with diffusion MRI in B6J mice.[24] Here, we present evidence that S6 mice also exhibit a significant ELM-RPE contraction in response to ACZ. In addition, we note that ELM-RPE and MCP/AR appear to be independent indices since both strains show ELM-RPE thinning in response to ACZ but different strain-dependent MCP/AR responses. Together, ELM-RPE contraction supports the notion that ACZ-induced acidification, but this thinning of the ELM-RPE did not seem to contribute to the ACZ-evoked changes observed in MCP/AR.

In this study, we also show ACZ caused a reduction in HB intensity, a correlate with ELM-RPE thickness.[23] This result is in apparent conflict from our earlier OCT study which suggested that the HB intensity was insensitive to ACZ.[5,23,25] We speculate that the different outcomes result from the different experimental designs of the two studies – longitudinal in the earlier study and cross-sectional in this study. In the longitudinal design, baseline scans for each mouse were obtained in light-dark conditions and, after a 3-day rest, were scanned again in light-dark conditions after receiving ACZ.[23] Thus, the same mouse was handled, anesthetized, and recovered more times than with the present cross-sectional design. It is unclear if more procedures/handling in the longitudinal design led to greater physiologic and/or metabolic stress than in the cross-sectional design and whether this additional stress may have contributed to lack

of an ACZ-induced changes in the HB intensity. More work is needed to test this hypothesis. It is also possible that higher signal-to-noise images used in the present study compared to the earlier study facilitated observation of the HB changes with ACZ. In any event, the present results may provide an explanation for why the HB band is much smaller in S6 mice: they have more efficient and active mitochondria producing a lower pH – thus a smaller HB intensity – than B6J mice.[10] Another possibility, that the smaller HB band in S6 mice may be a result of insufficient resolution, is ruled out because the OCT axial resolution is the same for B6J and S6 mice, and these two strains have retina's with similar laminar thicknesses (see Supplementary Material here[21]). In support of the notion that S6 mice have a lower subretinal space pH, we note that the ELM-RPE region is more contracted in light-adapted S6 mice than in B6J mice.[10,43]

One unexpected finding in this study is that ACZ evoked thinning of the outer nuclear layer in both B6J and S6 mice, and of the inner nuclear layer only in B6J mice (see Fig. 3). Because ONL thinning was seen in 1 hour of light adapted but not 5 hours in light adapted B6J mice, it seems unlikely that this thinning represents degeneration and we instead focused on changes in hydration. One potential mechanism involves aquaporin-1, a water channel that contributes to ionic and osmotic balance that is expressed in both nuclear layers.[44] However, contradictory evidence in the literature provides an unclear picture of whether ACZ can inhibit aquaporin-1 activity.[45,46] Alternatively, ACZ-sensitive carbonic anhydrase is present in Mueller cells – glia that play an important role in water removal of the nuclear layers.[47] For these reasons, we suspect that nuclear layer thinning is due to increased water removal from the nuclear layers and not overt degeneration; ACZ is an approved drug that is considered safe.[27,48,49] Further investigations will be useful in clarifying the role of Mueller cells – which contribute to nuclear layer hydration – in the ACZ-sensitive nuclear layer thinning.[50]

We note limitations of the present work. First, ACZ responses were studied in male mice only and studies in female mice are needed. In addition, more work is needed to test whether the strain-dependent MCP/AR changes in response to ACZ have the predicted consequences such as being pro-survival and/or are associated with changes in outer retina oxygen consumption rates. However, measuring the outer retina oxygen consumption rate in mice is technically challenging. It has been reported only once in a single paper by a single group in 2006 in vivo with oxygen electrodes; ACZ provocation was not part of that study.[51] Further, most oxygen consumption rate (OCR) measurements to-date, including in a previous paper of ours, have been performed on excised whole retina, a method that does not separate out inner from outer retina OCR, a likely complication of any interpretation of how ACZ specifically impacts the avascular outer retina OCR.[10,30,31] We note that although ACZ evokes an increase in cerebral and choroidal flow, most studies conclude that the cerebral metabolic rate of oxygen metabolism is unchanged by ACZ.[52,53] These results question the link between increased blood flow and increased oxygen consumption rates. Finally, we note that any potential bias in MCP/AR due to noise requires further investigation. Noise-bias has been discussed in the limit of a very weak OCT signal to account for any small meaningful signal contribution sitting on top of a comparatively large noise floor.[54] Thus, it is possible a reduced MCP/AR becomes susceptible to a noise-bias. Our statistical analyses did not find evidence that a noise-bias was a concern in this study because the effects of noise are encoded into the variance of each measurement and considered statistically using linear-mixed modeling; it can be also be appreciated that the variance in the MCP/AR values in S6 mice following ACZ (the smallest MCP/AR in this study) are not visibly greater than in any of the other groups. Nonetheless, more work is needed to test for, and possibly correct, a noise-bias contribution.

In summary, evidence provided by this study suggests a noninvasive test of photoreceptor mitochondria performance by combining OCT with an ACZ challenge. This approach may provide novel information about rod mitochondria injury, a mechanism which commonly contributes prodromally to sight threatening retinopathies that involve subretinal space acidification, such as diabetic retinopathy.[12,22,55–59] It has been unclear how to translate results from ex vivo studies to the clinic given the diversity in patient genetics and mitochondria pathophysiology. An OCT + ACZ challenge may allow personalized evaluation and treatment response of rod mitochondria dysfunction in patients.

Disclosure: **B.A. Berkowitz**, None; **A. Paruchuri**, None; **J. Stanek**, None; **R.H. Podolsky**, None; **K.L. Childers**, None; **R. Roberts**, None

References

1. Hoang QV, Linsenmeier RA, Chung CK, Curcio CA. Photoreceptor inner segments in monkey and human retina: mitochondrial density, optics, and regional variation. *Vis Neurosci*. 2002;19(4):395–407.

2. Padnick-Silver L, Linsenmeier RA. Quantification of in vivo anaerobic metabolism in the normal cat retina through intraretinal pH measurements. *Vis Neurosci*. 2002;19(6):793–806.

3. Govardovskii VI, Li JD, Dmitriev AV, Steinberg RH. Mathematical model of TMA+ diffusion and prediction of light-dependent subretinal hydration in chick retina. *Invest Ophthalmol Vis Sci*. 1994;35(6):2712–2724.

4. Li JD, Govardovskii VI, Steinberg RH. Light-dependent hydration of the space surrounding photoreceptors in the cat retina. *Vis Neurosci*. 1994;11(4):743–752.

5. Wolfensberger TJ, Dmitriev AV, Govardovskii VI. Inhibition of membrane-bound carbonic anhydrase decreases subretinal pH and volume. *Doc Ophthalmol*. 1999;97(3–4):261–271.

6. Adijanto J, Banzon T, Jalickee S, Wang NS, Miller SS. CO2-induced ion and fluid transport in human retinal pigment epithelium. *J Gen Physiol*. 2009;133(6):603–622.

7. Bissig D, Berkowitz BA. Light-dependent changes in outer retinal water diffusion in rats in vivo. *Mol Vis*. 2012;18:2561–2xxx.

8. Berkowitz BA, Grady EM, Khetarpal N, Patel A, Roberts R. Oxidative stress and light-evoked responses of the posterior segment in a mouse model of diabetic retinopathy. *Invest Ophthalmol Vis Sci*. 2015;56(1):606–615.

9. Lu CD, Lee B, Schottenhamml J, Maier A, Pugh EN, Fujimoto JG. Photoreceptor layer thickness changes during dark adaptation observed with ultrahigh-resolution opti-

cal coherence tomography. *Invest Ophthalmol Vis Sci.* 2017;58(11):4632–4643.

10. Berkowitz BA, Podolsky RH, Qian H, et al. Mitochondrial respiration in outer retina contributes to light-evoked increase in hydration in vivo. *Invest Ophthalmol Vis Sci.* 2018;59(15):5957–64.

11. Berkowitz BA, Qian H. OCT imaging of rod mitochondrial respiration in vivo. *Exp Biol Med (Maywood, NJ).* 2021:15353702211013799.

12. Berkowitz BA. Preventing diabetic retinopathy by mitigating subretinal space oxidative stress in vivo. *Vis Neurosci.* 2020;37:E002.

13. Linsenmeier RA, Budzynski E, Chung CK, eds. The role of the pH microenvironment in retinal diseases. *Proceedings of the Second Joint 24th Annual Conference and the Annual Fall Meeting of the Biomedical Engineering Society] [Engineering in Medicine and Biology*; 2002: IEEE.

14. Yang Z, Alvarez BV, Chakarova C, et al. Mutant carbonic anhydrase 4 impairs pH regulation and causes retinal photoreceptor degeneration. *Human Molec Genet.* 2005;14(2):255–265.

15. Khacho M, Tarabay M, Patten D, et al. Acidosis overrides oxygen deprivation to maintain mitochondrial function and cell survival. *Nat Commun.* 2014;5:3550.

16. Dmitriev AV, Henderson D, Linsenmeier RA. Diabetes alters pH control in rat retina. *Invest Ophthalmol Vis Sci.* 2019;60(2):723–730.

17. Berdahl JP, Leske DA, Fautsch MP, Lanier WL, Holmes JM. Effect of bicarbonate on retinal vasculature and acidosis-induced retinopathy in the neonatal rat. *Graefes Arch Clin Exp Ophthalmol.* 2005;243(4):367–373.

18. Zhang S, Leske DA, Lanier WL, Berkowitz BA, Holmes JM. Preretinal neovascularization associated with acetazolamide-induced systemic acidosis in the neonatal rat. *Invest Ophthalmol Vis Sci.* 2001;42(5):1066–1071.

19. Holmes JM, Zhang S, Leske DA, Lanier WL. Metabolic acidosis-induced retinopathy in the neonatal rat. *Invest Ophthalmol Vis Sci.* 1999;40(3):804–809.

20. Datta R, Waheed A, Bonapace G, Shah GN, Sly WS. Pathogenesis of retinitis pigmentosa associated with apoptosis-inducing mutations in carbonic anhydrase IV. *Proc Natl Acad Sci.* 2009;106(9):3437–3442.

21. Berkowitz BA, Podolsky RH, Childers KL, et al. Functional changes within the rod inner segment ellipsoid in wild-type mice: an optical coherence tomography and electron microscopy study. *Invest Ophthalmol Vis Sci.* 2022;63(8):8.

22. Berkowitz BA, Podolsky RH, Childers KL, et al. Transducin-deficient rod photoreceptors evaluated with optical coherence tomography and oxygen consumption rate energy biomarkers. *Invest Ophthalmol Vis Sci.* 2022;63(13):22.

23. Gao S, Li Y, Bissig D, et al. Functional regulation of an outer retina hyporeflective band on optical coherence tomography images. *Sci Rep.* 2021;11(1):10260.

24. Berkowitz BA, Bissig D, Roberts R. MRI of rod cell compartment-specific function in disease and treatment in-ávivo. *Prog Retinal Eye Res.* 2016;51:90–106.

25. Yamamoto F, Steinberg RH. Effects of intravenous acetazolamide on retinal pH in the cat. *Exp Eye Res.* 1992;54(5):711–718.

26. Findl O, Hansen RM, Fulton AB. The effects of acetazolamide on the electroretinographic responses in rats. *Invest Ophthalmol Vis Sci.* 1995;36(6):1019–1026.

27. Vagal AS, Leach JL, Fernandez-Ulloa M, Zuccarello M. The acetazolamide challenge: techniques and applications in the evaluation of chronic cerebral ischemia. *AJNR Am J Neuroradiol.* 2009;30(5):876–884.

28. Rassam SM, Patel V, Kohner EM. The effect of acetazolamide on the retinal circulation. *Eye.* 1993;7(Pt 5):697–702.

29. Ronchi JA, Figueira TR, Ravagnani FG, Oliveira HC, Vercesi AE, Castilho RF. A spontaneous mutation in the nicotinamide nucleotide transhydrogenase gene of C57BL/6J mice results in mitochondrial redox abnormalities. *Free Radic Biol Med.* 2013;63:446–456.

30. Medrano CJ, Fox DA. Oxygen consumption in the rat outer and inner retina: light- and pharmacologically-induced inhibition. *Exp Eye Res.* 1995;61(3):273–284.

31. Kooragayala K, Gotoh N, Cogliati T, et al. Quantification of oxygen consumption in retina ex vivo demonstrates limited reserve capacity of photoreceptor mitochondria. *Invest Ophthalmol Vis Sci.* 2015;56(13):8428–36.

32. Berkowitz BA, Podolsky RH, Lenning J, et al. Sodium iodate produces a strain-dependent retinal oxidative stress response measured in vivo using QUEST MRI. *Invest Ophthalmol Vis Sci.* 2017;58(7):3286–3293.

33. Berkowitz BA, Lewin AS, Biswal MR, Bredell BX, Davis C, Roberts R. MRI of retinal free radical production with laminar resolution in vivo. *Invest Ophthalmol Vis Sci.* 2016;57(2):577–585.

34. Berkowitz BA, Bredell BX, Davis C, Samardzija M, Grimm C, Roberts R. Measuring in vivo free radical production by the outer retina. *Invest Ophthalmol Vis Sci.* 2015;56(13):7931–7938.

35. DeRamus ML, Stacks DA, Zhang Y, Huisingh CE, McGwin G, Pittler SJ. GARP2 accelerates retinal degeneration in rod cGMP-gated cation channel β-subunit knockout mice. *Sci Rep.* 2017;7:42545.

36. Soukup P, Maloca P, Altmann B, Festag M, Atzpodien EA, Pot S. Interspecies variation of outer retina and choriocapillaris imaged with optical coherence tomography. *Invest Ophthalmol Vis Sci.* 2019;60(10):3332–3342.

37. Zhang T, Kho AM, Yiu G, Srinivasan VJ. Visible light optical coherence tomography (OCT) quantifies subcellular contributions to outer retinal band 4. *Transl Vis Sci Technol.* 2021;10(3):30.

38. Berkowitz BA, Olds HK, Richards C, et al. Novel imaging biomarkers for mapping the impact of mild mitochondrial uncoupling in the outer retina in vivo. *PLoS One.* 2020;15(1):e0226840.

39. Berkowitz BA, Podolsky RH, Childers KL, et al. Rod photoreceptor neuroprotection in dark-reared Pde6brd10 mice. *Invest Ophthalmol Vis Sci.* 2020;61(13):14-.

40. Mulchrone KF, Choudhury KR. Fitting an ellipse to an arbitrary shape: implications for strain analysis. *J Structur Geol.* 2004;26(1):143–153.

41. Berkowitz BA, Podolsky RH, Childers KL, Roberts R, Waseem R. Multiple bioenergy-linked OCT biomarkers suggest greater-than-normal rod mitochondria activity early in experimental Alzheimer's disease. *Invest Ophthalmol Vis Sci.* 2023;64(3):12.

42. Yamamoto F, Borgula GA, Steinberg RH. Effects of light and darkness on pH outside rod photoreceptors in the cat retina. *Exp Eye Res.* 1992;54(5):685–697.

43. Bringmann A, Pannicke T, Grosche J, el al. Müller cells in the healthy and diseased retina. *Prog Retin Eye Res.* 2006;25(4):397–424.

44. Kang TH, Choi YK, Kim IB, Oh SJ, Chun MH. Identification and characterization of an aquaporin 1 immunoreactive amacrine-type cell of the mouse retina. *J Compar Neurol.* 2005;488(3):352–367.

45. Yang B, Kim JK, Verkman A. Comparative efficacy of HgCl2 with candidate aquaporin-1 inhibitors DMSO, gold, TEA+ and acetazolamide. *FEBS Lett.* 2006;580(28-29):6679–6684.

46. Gao J, Wang X, Chang Y, et al. Acetazolamide inhibits osmotic water permeability by interaction with aquaporin-1. *Analytic Biochem*. 2006;350(2):165–170.

47. Newman EA. A physiological measure of carbonic anhydrase in Müller cells. *Glia*. 1994;11(4):291–299.

48. Larsson LI, Alm A. Aqueous humor flow in human eyes treated with dorzolamide and different doses of acetazolamide. *Arch Ophthalmol*. 1998;116(1):19–24.

49. Cox SN, Hay E, Bird AC. Treatment of chronic macular edema with acetazolamide. *Arch Ophthalmol*. 1988;106(9):1190–1195.

50. Reichenbach A, Wurm A, Pannicke T, Iandiev I, Wiedemann P, Bringmann A. Muller cells as players in retinal degeneration and edema. *Graefes Arch Clin Exp Ophthalmol*. 2007;245(5):627–636.

51. Yu DY, Cringle SJ. Oxygen distribution in the mouse retina. *Invest Ophthalmol Vis Sci*. 2006;47(3):1109–1112.

52. Buch S, Ye Y, Haacke EM. Quantifying the changes in oxygen extraction fraction and cerebral activity caused by caffeine and acetazolamide. *J Cereb Blood Flow Metab*. 2017;37(3):825–836.

53. Okazawa H, Yamauchi H, Sugimoto K, Toyoda H, Kishibe Y, Takahashi M. Effects of acetazolamide on cerebral blood flow, blood volume, and oxygen metabolism: a positron emission tomography study with healthy volunteers. *J Cereb Blood Flow Metab*. 2001;21(12):1472–1479.

54. Baumann B, Merkle CW, Leitgeb RA, et al. Signal averaging improves signal-to-noise in OCT images: but which approach works best, and when? *Biomed Opt Express*. 2019;10(11):5755–5775.

55. Sivapathasuntharam C, Sivaprasad S, Hogg C, Jeffery G. Improving mitochondrial function significantly reduces the rate of age related photoreceptor loss. *Exp Eye Res*. 2019;185:107691.

56. Perron NR, Beeson C, Rohrer B. Early alterations in mitochondrial reserve capacity; a means to predict subsequent photoreceptor cell death. *J Bioenerg Biomembr*. 2013;45(0):101–109.

57. Du Y, Veenstra A, Palczewski K, Kern TS. Photoreceptor cells are major contributors to diabetes-induced oxidative stress and local inflammation in the retina. *Proc Nat Acad Sci*. 2013;110(41):16586–16591.

58. Jiang K, Mondal AK, Adlakha YK, et al. Multiomics analyses reveal early metabolic imbalance and mitochondrial stress in neonatal photoreceptors leading to cell death in Pde6brd1/rd1 mouse model of retinal degeneration. *Hum Mol Genet*. 2022;31(13):2137–2154.

59. Mirra S, García-Arroyo R, Domenech EB, et al. CERKL, a retinal dystrophy gene, regulates mitochondrial function and dynamics in the mammalian retina. *Neurobiol Dis*. 2021;156:105405.